

# Contents

<b>1</b>	<b>Introduction</b>	<b>1</b>
<b>2</b>	<b>Theory of Operation</b>	<b>1</b>
2.1	Cascaded-Coupler Technique (Perfectly Matched Condition) . . . . .	1
2.2	Effect of Impedance Mismatch on the Cascaded-Coupler Equation . . . . .	3
2.2.1	Effect of Coupler Removal on Mismatch . . . . .	3
2.2.2	Mismatch Corrected Cascading Equation . . . . .	4
<b>3</b>	<b>System Design</b>	<b>6</b>
3.1	Hardware . . . . .	6
3.2	Software . . . . .	8
<b>4</b>	<b>Uncertainty Analysis</b>	<b>8</b>
4.1	Type A Uncertainty . . . . .	9
4.2	Type B Uncertainty . . . . .	9
4.2.1	Fractional Uncertainty in the Bolometric Power Readings . . . . .	11
4.2.2	Uncertainty in the Determination of Mismatch . . . . .	11
4.2.3	Coupling Ratio Stability (Linearity) . . . . .	12
<b>5</b>	<b>Comparison Test Results and Summary</b>	<b>12</b>
	<b>References</b>	<b>15</b>

# Switched-Coupler Measurements for High-Power RF Calibrations

J. Wayde Allen  
National Institute of Standards and Technology  
325 Broadway  
Boulder, Colorado 80303

This paper describes the design and operational theory behind the new high-power measurement system recently developed at the National Institute of Standards and Technology (NIST). This new system makes use of the established low power bolometer calibration service, and extends our measurement capability up to 1 kW in the 2 MHz to 1000 MHz frequency range.

**Keywords:** Microcalorimeter; Microwave Calorimeter; Microwave Power Measurement; Microwave Power Standard Waveguide; Microwave Power Standard

## 1 Introduction

In order to meet the demand for higher power calibrations, a new high-power measurement system had to be developed. The ‘Cascaded-Coupler’ technique, originally discussed by Kenneth Bramall in 1971 [1], was chosen for its ability to achieve an acceptable uncertainty at minimum cost. Specifically, it allows us to transfer the calibration of a bolometer mount measured on the existing microcalorimeter system to 1 kW with measurement uncertainties on the order of 2 %.

## 2 Theory of Operation

### 2.1 Cascaded-Coupler Technique (Perfectly Matched Condition)

In the cascaded coupler technique, the calibration of a low-power (10 mW) bolometric power sensor is sequentially transferred to similar sensors on the sidearms of a coupler chain as shown in Figure 1. The 10 dB coupler increment was chosen so that the bolometric sensors operate in the range from 1 mW to 10 mW. This is the range over which these sensors in combination with the NIST Type IV power meter have the lowest measurement uncertainty [2].

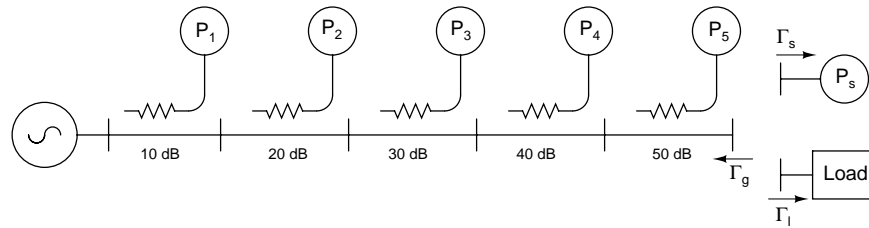


Figure 1: Series directional coupler chain.

Calibration of the coupler chain begins by connecting the calibrated sensor to the output port of the coupler chain and adjusting the power until this sensor reads 10 mW. The sensor on the sidearm of the 10 dB coupler should then read approximately 1 mW due to the 10 dB coupling ratio. It is now possible to determine the ratio between the reading on the calibrated sensor and that of the 10 dB sidearm. This calibrates the coupling ratio for the 10 dB coupler, and to the extent that the system is linear, the ratio will remain constant. For now, let us assume perfectly matched and linear conditions so that the effects of impedance mismatch and nonlinearity can be ignored.

Replacing the calibrated sensor with a matched load gives us

$$\frac{P_s}{P_1} = \frac{P_{l1}}{P_{1x}}, \quad (1)$$

where:

$P_s$  is the power delivered to the calibrated mount (approximately 10 mW),

$P_1$  is the power read from the 10 dB sidearm (approximately 1 mW),

$P_{l1}$  is the power delivered to the load, and

$P_{1x}$  is the 10 dB sidearm power with  $P_{l1}$  delivered to the load.

Solving eq. (1) for  $P_{l1}$  gives

$$P_{l1} = \frac{P_{1x}}{P_1} P_s. \quad (2)$$

If the power is now increased until the 10 dB coupler sidearm power reads approximately 10 mW, the power at the sidearm of the 20 dB coupler will be close to 1 mW. Forming a new set of ratios between the detectors on the 10 dB and 20 dB coupler sidearms results in

$$\frac{P_{l1}}{P_2} = \frac{P_{l2}}{P_{2x}}, \quad (3)$$

where:

$P_{l1}$  is the load power referenced to the 10 dB sidearm,

$P_2$  is the power reading on the 20 dB sidearm with 10 mW on the 10 dB sidearm,

$P_{l2}$  is the load power referenced to the 20 dB coupler sidearm, and

$P_{2x}$  is the 20 dB sidearm power with  $P_{l2}$  delivered to the load.

Substituting eq. (2) in place of  $P_{l1}$  and solving for  $P_{l2}$  gives

$$P_{l2} = \frac{P_{2x}}{P_2} \frac{P_{1x}}{P_1} P_s. \quad (4)$$

At this point, the 10 dB coupler is no longer needed, and *must* be physically removed from the coupler chain before the power is further increased. Increasing the power without removing the coupler will overload the power detector on the 10 dB coupler sidearm.

Increasing the power, forming the ratio of powers, and physically removing the lowest power coupler stage can be continued to extend the power calibration as far as needed. For the coupler chain diagrammed in Figure 1, the power equation for the final 50 dB coupler is

$$P_l = \frac{P_{5x}}{P_5} \frac{P_{4x}}{P_4} \frac{P_{3x}}{P_3} \frac{P_{2x}}{P_2} \frac{P_{1x}}{P_1} P_s. \quad (5)$$

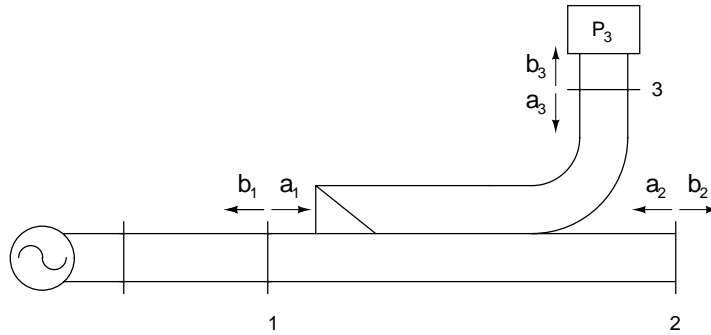


Figure 2: Single coupler circuit.

## 2.2 Effect of Impedance Mismatch on the Cascaded-Coupler Equation

In the preceding discussion it was assumed that all of the impedances are matched. In general they are not, and it is necessary to include a mismatch correction in the cascading equation. Because the mismatch correction depends on the equivalent generator reflection coefficient ( $\Gamma_g$ ) of the coupler chain, it is important to understand how removing couplers from the chain affects the measurement.

### 2.2.1 Effect of Coupler Removal on Mismatch

To understand the effect of coupler removal on the mismatch correction, the definition of  $\Gamma_g$  must be considered. This definition has been documented in several places by Glenn Engen [3][4, pp. 40–44], but can be summarized as follows.

Consider the circuit shown in Figure 2. If we take a look at the scattering parameter representation of the emergent wave amplitude  $b_2$  we get [4, eq. (6.5), p. 43]

$$b_2 = b_3 \left\{ \frac{S_{21}}{S_{31}} + \Gamma_d \left( S_{23} - \frac{S_{21}S_{33}}{S_{31}} \right) \right\} + a_2 \left( S_{22} - \frac{S_{21}S_{32}}{S_{31}} \right), \quad (6)$$

where  $\Gamma_d = a_3/b_3$ . Since we are not changing the coupler or the sensor, both the S-parameters and  $\Gamma_d$  are constant, and we can simplify the scattering parameter representation by writing it in the form

$$b_2 = b_3 S_{coupler} + a_2 \Gamma_g, \quad (7)$$

where  $\Gamma_g$  is the ‘equivalent’ reflection coefficient given by [4, eq. (6.6), p. 44]

$$\Gamma_g = S_{22} - \frac{S_{21}S_{32}}{S_{31}}, \quad (8)$$

and

$$S_{coupler} = \frac{S_{21}}{S_{31}} + \Gamma_d \left( S_{23} - \frac{S_{21}S_{33}}{S_{31}} \right). \quad (9)$$

In other words, the scattering parameter representation of the coupler can be replaced with the microwave equivalent of ‘Thevenin’s theorem’ [4, pp. 17–20] as in Figure 3.

Of particular interest is that  $\Gamma_g$  depends only on the internal characteristics of the directional coupler, not on anything that precedes the coupler. More importantly, the ratio of the power delivered to the coupler’s sidearm and the power delivered to its load are not affected by anything preceding the coupler.

Now note that during the initial calibration only the 10 dB coupler is used. The other couplers contribute only their insertion loss, so the entire chain can be thought of as one large 10 dB directional coupler as shown in Figure 4.

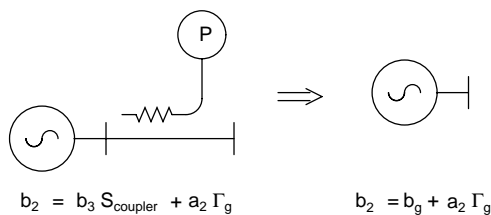


Figure 3: Equivalent generator representation of a directional coupler.

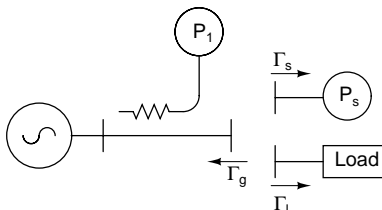


Figure 4: Equivalent circuit for first stage calibration.

Here the only  $\Gamma_g$  of interest is the one measured for the entire coupler chain referred to the 10 dB coupler sidearm and it can be used along with the values of  $\Gamma_s$  and  $\Gamma_l$  to compute the impedance mismatch between both  $P_s$  and the test load.

In the next step, transferring the calibration from the 10 dB coupler to the 20 dB coupler sidearm, the power is increased until we can read the power on the 20 dB sidearm. Nothing else is changed, but we now know how the power delivered to the load changes with respect to both the 10 dB and 20 dB sidearm powers. At this point, since the relationship between the 20 dB coupler sidearm power and the load power has been determined, the 10 dB coupler can be removed without affecting the calibration. The transfer to subsequent couplers continues in the same way; as long as the test load is not changed, only the initial mismatch conditions need to be considered.

### 2.2.2 Mismatch Corrected Cascading Equation

Since we are not able to construct a measurement system using perfect power sensors and perfect impedance matching between the components, eq. (2) must be modified to describe the more general condition. This is accomplished by noting that the level indicated by any of the power meters will only be the power delivered to the meter multiplied by the bolometer's effective efficiency ( $\eta$ ), so

$$P_{s_{meter}} = M_s \eta_s P_s, \quad (10)$$

$$P_{1_{meter}} = M_1 \eta_1 P_1, \quad (11)$$

$$P_{1x_{meter}} = M_1 \eta_1 P_{1x}, \quad (12)$$

where:

$P_{s_{meter}}$  is the DC substituted power reading on the meter connected to bolometer  $P_s$ ,

$M_s$  is the mismatch between the coupler chain and the bolometer mount  $P_s$ ,

$\eta_s$  is the effective efficiency of bolometer  $P_s$ ,

$P_s$  is the net power delivered to bolometer  $P_s$ ,

$P_{1_{meter}}$  the power indicated by the sidearm meter  $P_1$  with  $P_s$  attached,

$M_1$  the mismatch between the coupler sidearm and the bolometer  $P_1$ ,

$\eta_1$  the effective efficiency of meter  $P_1$ ,

$P_1$  is the net power delivered to meter  $P_1$ ,

$P_{1x_{meter}}$  the power indicated on meter  $P_1$  after attaching the load and increasing the system power, and

$P_{1x}$  is the net power delivered to meter  $P_1$  after attaching the the load and increasing the system power.

Similarly, the power delivered to the load is given by

$$P_{l_{delivered}} = M_l P_l, \quad (13)$$

where:

$P_l$  is the net power delivered to the load, and

$M_l$  is the mismatch between the coupler chain and the attached load.

If eq.s (10), (11), (12), and (13) are solved for the net delivered powers we get

$$P_s = \frac{P_{s_{meter}}}{M_s \eta_s}, \quad (14)$$

$$P_1 = \frac{P_{1_{meter}}}{M_1 \eta_1}, \quad (15)$$

$$P_{1x} = \frac{P_{1x_{meter}}}{M_1 \eta_1}, \quad (16)$$

$$P_l = \frac{P_{l_{delivered}}}{M_l}. \quad (17)$$

These equations can then be substituted into eq. (2) to get

$$P_{l_{delivered}} = \frac{P_{1x_{meter}}}{P_{1_{meter}}} \frac{M_l}{M_s} \frac{P_{s_{meter}}}{\eta_s}. \quad (18)$$

$M_l$  and  $M_s$  are defined [4, eq. (3.16), pp. 20–22] as

$$M_l = \frac{(1 - |\Gamma_l|^2)(1 - |\Gamma_g|^2)}{|1 - \Gamma_l \Gamma_g|^2} \quad (19)$$

and

$$M_s = \frac{(1 - |\Gamma_s|^2)(1 - |\Gamma_g|^2)}{|1 - \Gamma_s \Gamma_g|^2}. \quad (20)$$

Substituting these into eq. (18), and generalizing for multiple coupler stages, results in the corrected cascaded coupler equation

$$P_{l_{delivered}} = \frac{P_{nx_{meter}}}{P_{n_{meter}}} \cdots \frac{P_{2x_{meter}}}{P_{2_{meter}}} \frac{P_{1x_{meter}}}{P_{1_{meter}}} \frac{P_{s_{meter}}}{\eta_s} \frac{1 - |\Gamma_l|^2}{1 - |\Gamma_s|^2} \left| \frac{1 - \Gamma_s \Gamma_g}{1 - \Gamma_l \Gamma_g} \right|^2. \quad (21)$$

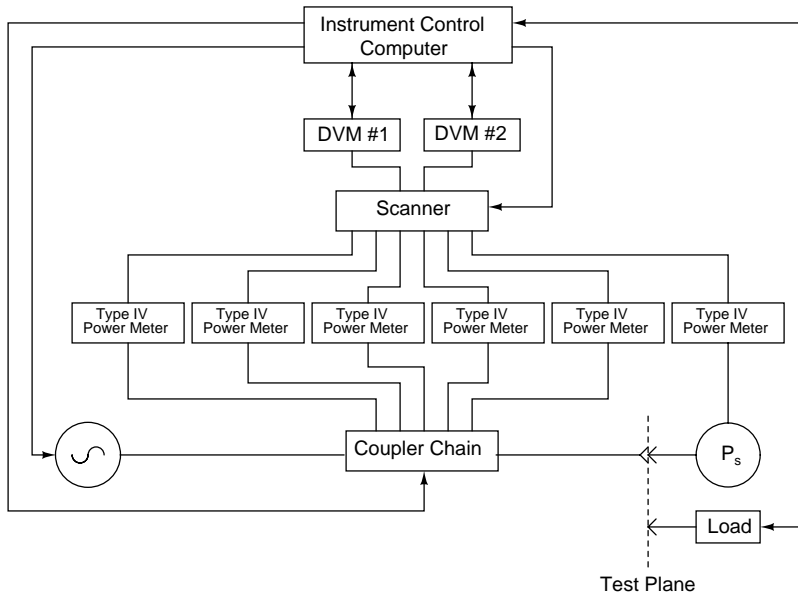


Figure 5: Block diagram of measurement system.

### 3 System Design

#### 3.1 Hardware

The previous discussion shows that the hardware requirements for the construction of a cascaded-coupler system are relatively modest. Only the couplers required to create the chain of couplers, power meters for the coupler sidearms, and an RF signal source capable of delivering the required power are needed. The coupler chain itself can be manually connected and the couplers removed as the measurement proceeds. This design works well for the occasional measurement, but is less attractive when a regular measurement program is anticipated. With this in mind, the system developed at NIST is designed to perform these functions under computer control.

Automating the measurement of the bolometer power levels is quite straight forward, and is achieved through the use of commercial digital voltmeters (DVMs), NIST Type IV power meters [2], and a commercial switch control unit or scanner. Figure 5 shows a block diagram of the system.

Two DVMs have been used to minimize the time difference between the power meter readings. Additionally, two Type IV power meters are connected to each bolometer mount. One of the power meters and the compensation element serve as a reference voltage generator (RVG). The other meter is connected to the RF measurement thermistors. This helps correct for thermal drift in the bolometer mount, and keeps the output voltage from the combined power meters in the DVMs most accurate operating range [5][2]. Figure 6 shows the wiring diagram for each bolometer. With this arrangement, we can read the voltage directly from the Type IV meter connected to the RF measurement bead by opening switch S2 and closing S1, or to read the voltage difference resulting from the series connection of both meters by opening S1 and closing S2.

Converting the DVM readings to RF power follows the procedure described by Fred Clague in NISTIR 5016 [5]. Switch S1 is initially closed and the voltage read with no RF power applied to get the initial zero power reading  $V_{1i}$  at time  $t_1$ . Next, switch S1 is opened and switch S2 is closed, giving a new off power voltage  $V_{1xi}$  with the series combination of the Type IV power meters at time  $t_2$ . The RF power is then turned on, and with switch S2 still closed the voltage  $V_{2x}$  is measured at time  $t_3$ . Then after the RF power has been turned off, the voltage of the series power meter combination  $V_{1xf}$  at time  $t_4$  is measured. Finally, switch S2 is opened and switch S1 closed. The final off-power voltage  $V_{1f}$  is then measured at time  $t_5$ . Combining

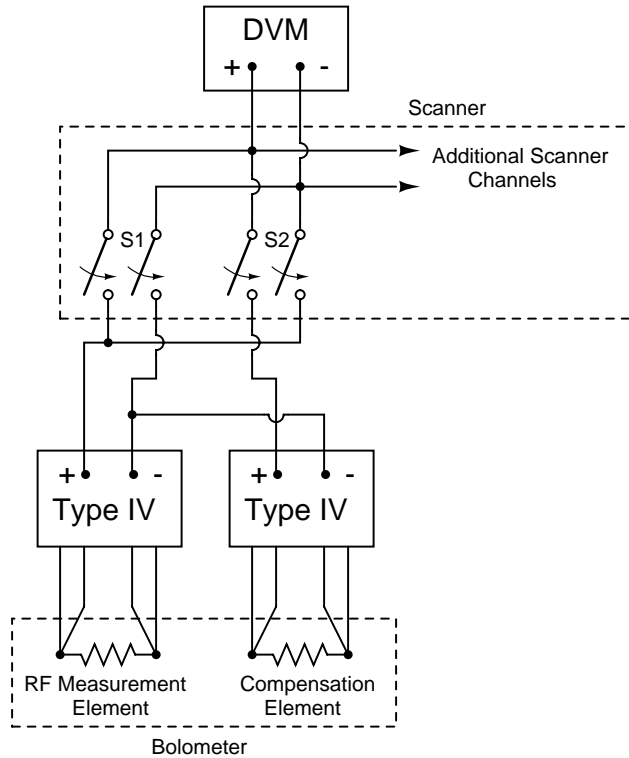


Figure 6: Power measurement circuit.

these measurements so that

$$V_1 = V_{1i} + \left( \frac{t_3 - t_1}{t_5 - t_1} \right) (V_{1f} - V_{1i}) \quad (22)$$

and

$$\Delta V = V_{2x} - \left[ V_{1xi} + \left( \frac{t_3 - t_2}{t_4 - t_2} \right) (V_{1xf} - V_{1xi}) \right] \quad (23)$$

provides the values needed for substitution into the Type IV power equation [5]

$$P = \frac{1}{K_b R_0} (2V_1 - \Delta V) \Delta V, \quad (24)$$

where  $R_0$  is the operating resistance of the mount, and  $K_b$  is the mount calibration factor.

Computer control of the cascaded-coupler chain is achieved using a matrix of RF switches connecting the couplers together as shown in Figure 7. This allows the computer to set the switches so that all the couplers are connected at the start of the measurement cycle and to remove the appropriate couplers as the power level is increased. The added insertion loss and power-handling capacity of the switches does, however, put a limit on the power that can be switched.

Typical insertion loss for high-power coaxial switches is on the order of 0.2 dB, so the inclusion of the eight switches shown in Figure 7 adds about 1.6 dB of loss to the coupler chain. Ignoring the insertion loss of the couplers themselves means that the RF source would need to supply nearly 1.5 kW in order to overcome the loss in the switching matrix. This exceeds the 1.1 kW power rating on the switches used, and the maximum power capability of our signal source. Simply excluding the final 50 dB coupler from the switching matrix minimizes this problem. With this arrangement, the operator manually connects the 50 dB coupler and calibrated bolometer  $P_s$  to the output of the switched coupler matrix before starting the measurement. The computer initializes the coupler matrix by connecting all of the couplers in series and measures the power ratio between  $P_s$  and  $P_1$  as described in Section 2. The operator then replaces  $P_s$  with the RF load, and the

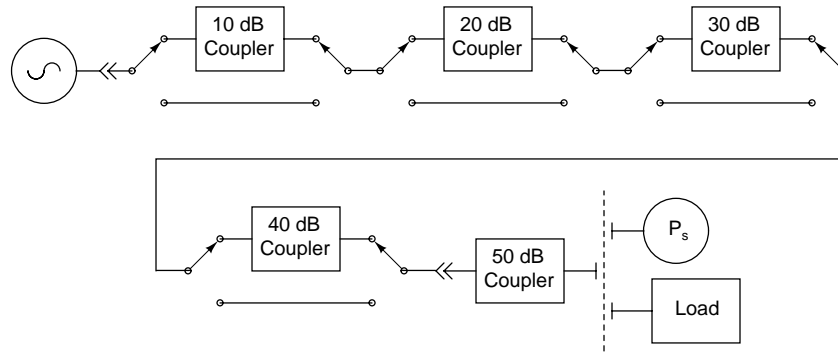


Figure 7: Switched coupler chain.

computer automatically transfers the power calibration down the chain. This sets up the calibration for the final 50 dB coupler, and is sufficient for power measurements up to 100 W. In this mode, the generator only needs to supply around 150 W to overcome the switch losses. To measure powers higher than 100 W, the operator simply disconnects the 50 dB coupler from the switched coupler matrix and reconnects it directly to the RF generator. The power can then be increased until 1000 W appears at the output of the 50 dB coupler, and assuming that the coupler has about 0.2 dB of insertion loss, the generator only needs to supply about 1050 W.

### 3.2 Software

The software for the measurement system was designed on the premise that it is easier to test, troubleshoot, and maintain several small programs rather than one very large program. This allows the code development to be split among the people working on the project and has the added benefit of the separate programs performing consistency checks on each other's data. For this project, the software was split into three main application groups: instrument control, data analysis, and report generation.

The instrument control program is the interface to the actual measurement hardware. It defines the measurement process and collects the data for final analysis. Only a minimal amount of computation such as the conversion of the Type IV DVM readings to RF power are done at this level. Data collected by the instrument control program are made available for subsequent processing as a pure ASCII file.

Data are analyzed by several Perl programs. One program formats these data into a more human-readable form (bramview) and another computes the Type B uncertainty (bramerr). Another program formats the output from the bramerr program into an ASCII grid suitable for importing into almost any spreadsheet program. This allows the results from a series of several measurement cycles to be collected together into a single spreadsheet, summarized, and the Type A uncertainty computed. The spreadsheet also facilitates the creation of a table of results that can be imported into a word processing program for the generation of the final report.

Ultimately, as we gain more experience with the idiosyncrasies of the system, the final data analysis and report generation functions may be automated. With the highly modular design of the systems data structure, adding this functionality or changing the analysis does not require a major rewrite of any large pieces of code with the subsequent danger of breaking the existing functionality.

## 4 Uncertainty Analysis

Following the conventions described in NIST Technical Note 1297 [6], the system uncertainty analysis is composed of three fundamental parts: Type A ( $U_a$ ), Type B ( $U_b$ ), and the expanded uncertainty ( $U$ ). Type A uncertainties are those based on any valid statistical method for data analysis. Type B uncertainties

are those determined by any other method. The expanded uncertainty is

$$U = 2\sqrt{U_a^2 + U_b^2}. \quad (25)$$

The following sections describe how the Type A and Type B components were determined for the cascaded coupler system.

## 4.1 Type A Uncertainty

The cascaded-coupler system is normally used to compare the power indicated by a high-power detector ( $P_{dut}$ ) to the calibrated power delivered to the detector by the coupler chain ( $P_l$ ). The ratio of these two powers

$$K = \frac{P_{dut}}{P_{delivered}} \quad (26)$$

is the calibration factor for the meter and can be computed at any arbitrary power during the calibration of the coupler chain. Since the calibration factor  $K$  is the value reported to the customer, this is the term that must ultimately be assigned an uncertainty.

In this case, we want to determine the Type A uncertainty by computing the standard deviation of the mean values of  $K$  determined at each power over at least three full calibrations of the cascaded coupler chain, or

$$U_a = \frac{1}{\sqrt{n}} \sqrt{\frac{\sum (K_i - K_{avg})^2}{n - 1}}, \quad (27)$$

where:

$U_a$  is the sample standard deviation of the calibration factor  $K$ ,

$K_i$  is the calibration factor for any single measurement,

$K_{avg}$  is the average calibration factor, and

$n$  is the number of measurements made.

One difficulty with this approach is that it assumes that between any two calibrations the measurement system can be reset to any given power. In practice, the power can only be reset to within several tens of watts. Fortunately, over this range the variation in  $K$  doesn't seem to be highly correlated with this variation in power. This indicates that a more complex multivariate statistical approach is not really warranted.

Instead, the fluctuation in power is simply ignored, and the average of the measured powers is reported. This effectively centers the reported value at the center of the cluster of data, and allows us to compute the random variation or Type A uncertainty of the calibration factor  $K$  as given by eq. (27). Figure 8 shows how the reported value of  $K$  and its Type A uncertainty compare for a typical set of data.

## 4.2 Type B Uncertainty

Several modifications to eq. (21) simplify the Type B uncertainty analysis. First, we can group the reflection coefficient terms together to define a general mismatch term

$$M = \frac{1 - |\Gamma_l|^2}{1 - |\Gamma_s|^2} \left| \frac{1 - \Gamma_g \Gamma_s}{1 - \Gamma_g \Gamma_l} \right|^2, \quad (28)$$

and, second, we can define

$$P'_s = \frac{P_{s\,meter}}{\eta_s}. \quad (29)$$

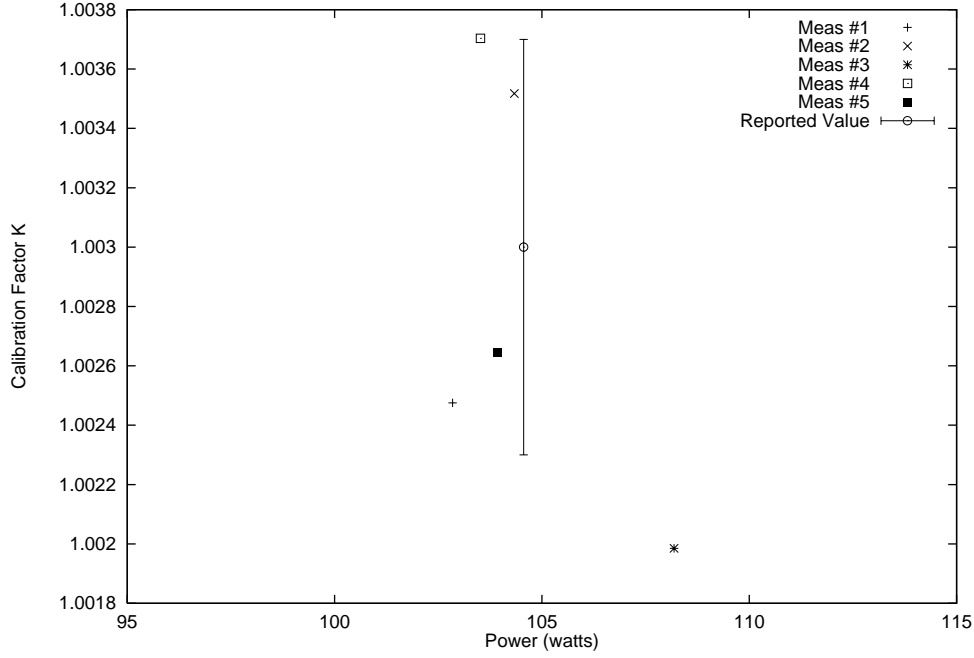


Figure 8: The reported calibration factor  $K$  and its Type A uncertainty for a typical raw data set.

This allows us to write the solution for the first coupler stage as

$$P_{l1\text{delivered}} = \frac{P_{1x\text{meter}}}{P_{1\text{meter}}} P'_s M. \quad (30)$$

Next, taking the partial derivatives for each of the terms in eq. (30) and computing the fractional change in  $P_{l1\text{delivered}}$  results in the expression

$$\frac{\Delta P_{l1\text{delivered}}}{P_{l1\text{delivered}}} = \frac{\Delta P_{1x\text{meter}}}{P_{1x\text{meter}}} + \frac{\Delta P_{1\text{meter}}}{P_{1\text{meter}}} + \frac{\Delta P'_s}{P'_s} + \frac{\Delta M}{M}. \quad (31)$$

An additional uncertainty term can be found by noting that eq. (21) assumes the directional couplers used in the system are linear. That means that the coupling ratio

$$C_1 = \frac{P'_s}{P_{1\text{meter}}} \quad (32)$$

should be constant. Equation (32) can be substituted into eq. (30) to get

$$P_{l1\text{delivered}} = P_{1x\text{meter}} C_1 M, \quad (33)$$

which indicates that the fractional change in  $P_{l1\text{delivered}}$  due to a change in the coupling ratio is  $\Delta C_1/C_1$ . Adding this coupler nonlinearity term to eq. (31) gives us an expression for the fractional uncertainty due to the first coupler stage

$$\frac{\Delta P_{l1\text{delivered}}}{P_{l1\text{delivered}}} = \frac{\Delta P_{1x\text{meter}}}{P_{1x\text{meter}}} + \frac{\Delta P_{1\text{meter}}}{P_{1\text{meter}}} + \frac{\Delta P'_s}{P'_s} + \frac{\Delta M}{M} + \frac{\Delta C_1}{C_1}. \quad (34)$$

The solution for the second stage equation can be written in terms of eq. (30) as

$$P_{l2\text{delivered}} = \frac{P_{2x\text{meter}}}{P_{2\text{meter}}} P_{l1\text{delivered}}. \quad (35)$$

The approach used to derive eq. (31) is then applied to eq. (35) to obtain

$$\frac{\Delta P_{l2_{delivered}}}{P_{l2_{delivered}}} = \frac{\Delta P_{2x_{meter}}}{P_{2x_{meter}}} + \frac{\Delta P_{2_{meter}}}{P_{2_{meter}}} + \frac{\Delta C_2}{C_2} + \frac{\Delta P_{l1_{delivered}}}{P_{l1_{delivered}}}, \quad (36)$$

where  $C_2$  is fractional change in the coupling ratio for the second directional coupler. Equation (36) can further be generalized so that the total uncertainty of any stage following the first one can be written as

$$\frac{\Delta P_{ln_{delivered}}}{P_{ln_{delivered}}} = \frac{\Delta P_{nx_{meter}}}{P_{nx_{meter}}} + \frac{\Delta P_{n_{meter}}}{P_{n_{meter}}} + \frac{\Delta C_n}{C_n} + \frac{\Delta P_{l(n-1)_{delivered}}}{P_{l(n-1)_{delivered}}}. \quad (37)$$

Referring back to eq. (26) we note that the calibration factor  $K$  only depends on the two values  $P_{dut}$  and  $P_{l_{delivered}}$ . Since for any given measurement,  $P_{dut}$  is just the power read off the customer's device, the uncertainty  $U_b$  only depends on the uncertainty in  $P_{l_{delivered}}$ , or

$$U_b = \frac{\Delta P_{ln_{delivered}}}{P_{ln_{delivered}}}. \quad (38)$$

We assume a rectangular distribution for each of the terms in  $U_b$ .

All that remains is to find accurate estimates for each of the uncertainty terms:

- The fractional uncertainty in the bolometric power readings ( $\Delta P'_s/P'_s$  and  $\Delta P_n/P_n$ ),
- The fractional uncertainty in the mismatch term ( $\Delta M/M$ ), and
- The coupling ratio stability or nonlinearity term ( $\Delta C_n/C_n$ ).

#### 4.2.1 Fractional Uncertainty in the Bolometric Power Readings

The calibrated power  $P'_s$  is determined from the DC substituted power indicated by the Type IV power meter and the calibrated value of the mount's effective efficiency ( $\eta_s$ ) as

$$P'_s = \frac{P_{s_{meter}} \pm \Delta P_{s_{meter}}}{\eta_s \pm \Delta \eta_s}. \quad (39)$$

Consequently, the uncertainty in the value of  $P'_s$  is

$$\Delta P'_s = \sqrt{\Delta P_{s_{meter}}^2 + \Delta \eta_s^2}. \quad (40)$$

The value  $\Delta \eta_s$  comes from the calibration of the mount  $P_s$ . The value for  $\Delta P_{s_{meter}}$  is computed from the uncertainties in the Type IV power meter and the voltmeter used to read the bias voltages. This computation has been coded directly into the software used to compute the DC substituted power since the raw power meter voltages are most readily accessible at this level. The computation of the DC-substituted power uncertainty when using the NIST Type IV power meter is covered in references [2] and [7].

For the power measurements made on the coupler sidearms, a correction for effective efficiency is not needed since these mounts are calibrated 'in place' against the mount  $P_s$ . Only the measured DC substituted power uncertainty need be considered.

#### 4.2.2 Uncertainty in the Determination of Mismatch

Measurement of the reflection coefficients  $\Gamma_l$ ,  $\Gamma_s$ , and  $\Gamma_g$  are made using either a vector network analyzer (VNA) or six-port network analyzer. The resulting uncertainties are on the order of 0.005 in the real and imaginary components. The uncertainty analysis software (bramerr) computes the mismatch from the measured reflection coefficients  $\Gamma_l$ ,  $\Gamma_s$ , and  $\Gamma_g$ , and the 64 possible variations in the mismatch due to the addition or subtraction of 0.005 from the real and imaginary components. The maximum difference between  $M$  and one of the 64 mismatch variants is used as the mismatch uncertainty  $\Delta M$ .

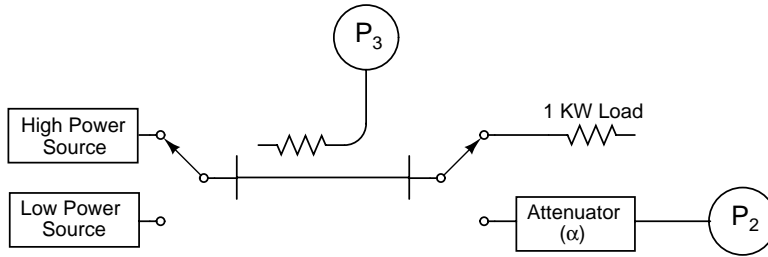


Figure 9: Test setup for determining coupler non-linearity

### 4.2.3 Coupling Ratio Stability (Linearity)

Equation (21) assumes that the system is linear and that the measured power ratios are constant. Unfortunately the world is not perfect and we need to allow for the possibility that the ratios depend on power.

A direct measurement of the power coupling ratio is not possible because it would exceed the dynamic range of the available power sensors and is the reason for building the cascaded coupler system in the first place. However, assuming that changes in the coupling ratio are most likely caused by thermal expansion in the coupler, we can design an experiment to get a reasonable estimate for the uncertainty due to coupler nonlinearity.

The setup used for determining coupler nonlinearity is shown in Figure 9. The switches can be set so that a low power source can deliver a signal that can be sampled by both power detectors  $P_3$  and  $P_2$ . The attenuation factor ( $\alpha$ ) is chosen so that the detectors  $P_3$  and  $P_2$  are operating within their normal operating range and is assumed to be constant. These powers can then be used to compute the coupling ratio

$$C = \frac{P_3 \alpha}{P_2}. \quad (41)$$

Setting the switches so that the output of the coupler is connected to the 1 kW load and applying a high power signal heats the coupler with the RF in the same manner in which it is used in the coupler chain. The powers  $P_3$  and  $P_2$  can be remeasured on the ‘hot’ coupler by turning off the ‘heating’ power and immediately resetting the switches to the low power circuit. The fractional uncertainty due to coupler nonlinearity is then

$$\frac{\Delta C}{C} = \left| \frac{C_{hot} - C_{cold}}{C_{cold}} \right|, \quad (42)$$

where  $C_{cold}$  is the coupling ratio measured before applying the heating power, and  $C_{hot}$  is the resulting measurement afterwards.

Tests done on water-cooled couplers gave us values for the fractional uncertainty ranging from 0.00008 to about 0.0005. Since this is such a small value, I decided that creating a separate uncertainty for each coupler was not worth the extra effort. The maximum value of 0.0005 was chosen as being a reasonable estimate of the fractional uncertainty due to nonlinearity in each coupler stage.

## 5 Comparison Test Results and Summary

To ensure continuity between the new switched-coupler measurement system and the older, low-frequency Bramall system [8], comparison measurements were done on a feed-through wattmeter. Figure 10 shows how these two systems compare at 30 MHz. This is the only point where we have measurement data up to 1000 W on the low frequency system. The figure shows that there is good agreement between both measurement systems.

Table 1 shows a representative set of data taken with the new measurement system. The  $\Delta P/P$  uncertainty is the sum of the power ratio uncertainties given in eq. (37).

Table 1: Table of typical measurement data.

Frequency (MHz)	Power (W)	$\frac{\Delta P}{P}$ (%)	$\frac{\Delta M}{M}$ (%)	$\frac{\Delta C}{C}$ (%)	$K$ (%)	$U_a$ (%)	$U_b$ (%)	$U$ (%)
550	0.572	0.05	0.24	0.10	0.992	0.71	0.40	1.63
550	13.525	0.08	0.24	0.15	1.003	0.83	0.47	1.91
550	93.424	0.10	0.24	0.20	1.019	0.79	0.54	1.92
550	993.854	0.12	0.24	0.25	1.025	0.82	0.61	2.04

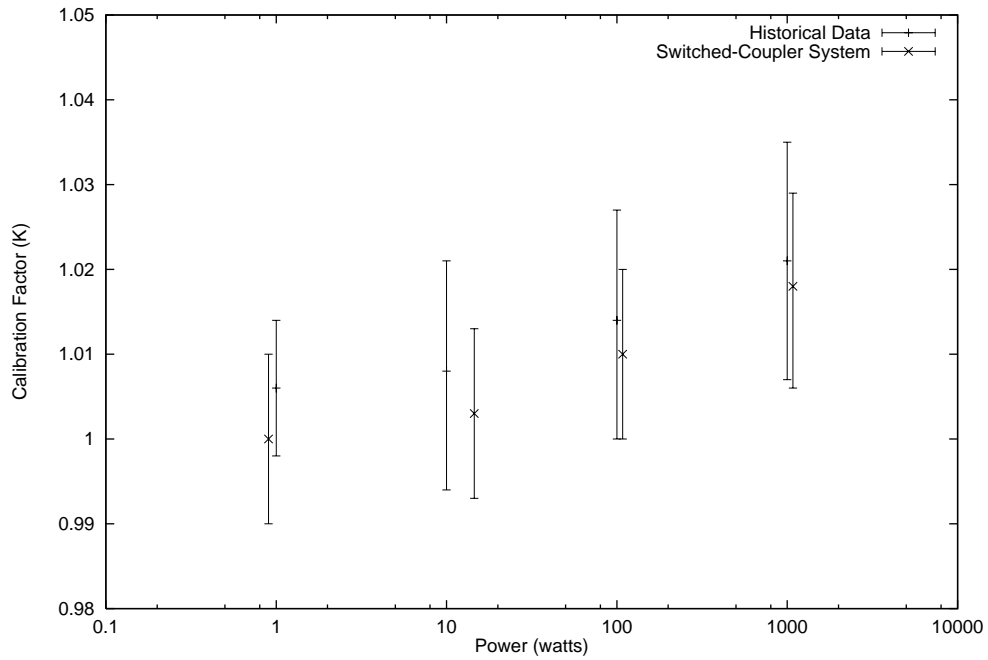


Figure 10: Comparison of historical calibration data with the new switched-coupler system at 30 MHz.

As shown here, typical uncertainties lie between 1 and 2 %. We do see some degradation of the system uncertainty at frequencies around 850 MHz and higher caused by a decrease in repeatability between multiple calibrations of the coupler chain. However, this could be due to increased amplifier noise. Work is continuing in an attempt to reduce the random uncertainty in the higher frequency bands.

## References

- [1] Bramall, K. E. Accurate microwave high power measurements using a cascaded coupler method. *Journal of Research of the National Bureau of Standards*, 75C(3 and 4):185–192; July–December 1971.
- [2] Larsen, N. T. A new self-balancing DC-substitution RF power meter. *IEEE Transactions on Instrumentation and Measurement*, IM-25, 4:28–32; December 1976.
- [3] Engen, G. F. Amplitude stabilization of a microwave signal source. *IRE Transactions on Microwave Theory and Techniques*, MTT-6, pp. 202-206; April 1958.
- [4] Engen, G. F. *Microwave Circuit Theory and Foundations of Microwave Metrology*. IEEE Electrical Measurement Series 9. Peter Peregrinus Ltd., London, United Kingdom; 1992.
- [5] Clague, F. NIST model PM2 power measurement system for 1 mW at 1 GHz. NISTIR 5016, National Institute of Standards and Technology; December 1993.
- [6] Taylor, B. N.; Kuyatt, C. E. Guidelines for evaluating and expressing the uncertainty of NIST measurement results. Technical Note 1297, National Institute of Standards and Technology; 1994.
- [7] Larsen, N. T. NBS Type IV RF power meter operation and maintenance. NBSIR 77-866, U.S. National Bureau of Standards; October 1977.
- [8] Rebuldela, G.; Jargon, J. A. High power CW wattmeter calibration at NIST. *Journal of Research of the National Institute of Standards and Technology*, 97(6):673–687; November–December 1992.